ON-FIBER DIELECTRIC METASURFACE FOR DYNAMIC POLARIZATION MANIPULATION: SUPPLEMENTAL DOCUMENT

S1. Design principle of phase profiles on DP-MS.

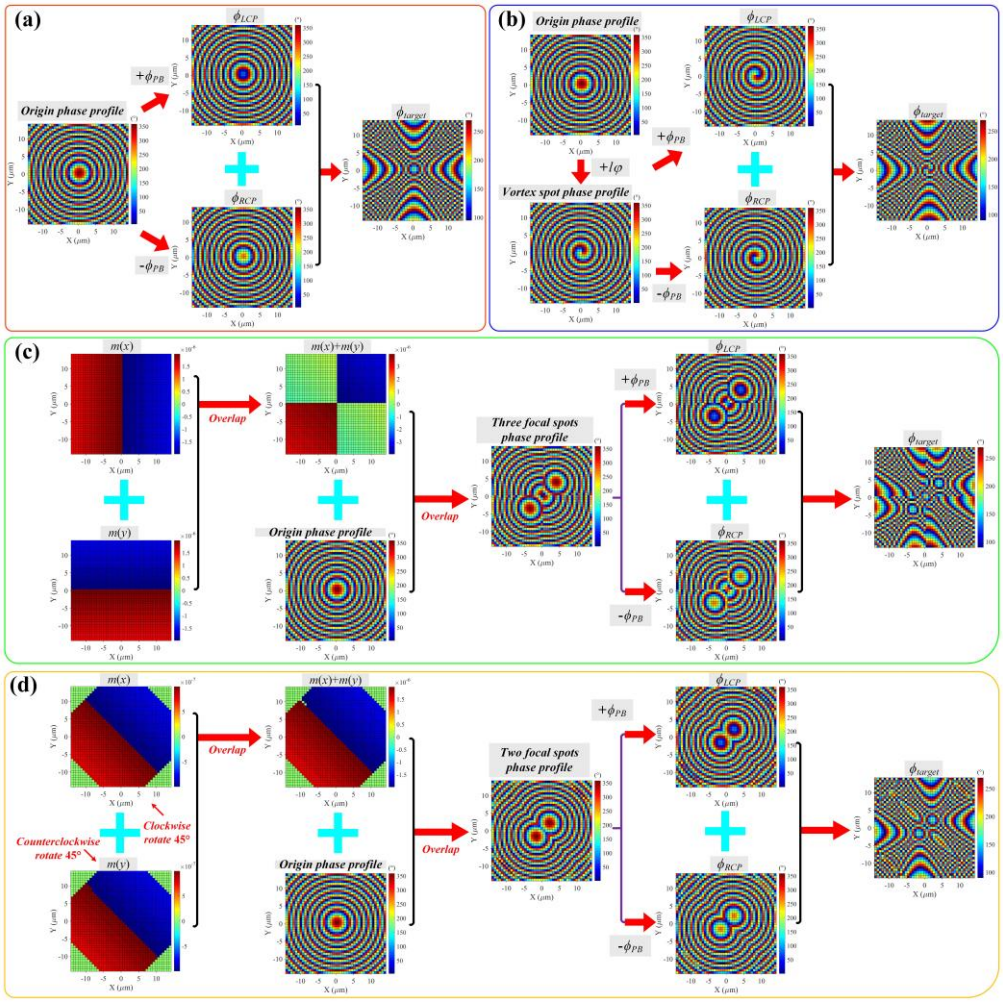

Fig. S1. Design principle of phase profiles on DP-MS: (a) single focal spot; (b) vortex spot; multi-focal fields generated by overlapping different sawtooth waves: (c) rotation angle $\theta = 0°$, amplitude $A = 2$ μm and (d) rotation angle $\theta = 45°$, amplitude $A = 1$ μm.

To gain a deeper understanding of how different DP-MS generate focal spots, we present a detailed explanation of the phase profile design principle. As shown in Fig. S1(a), the original phase profile is combined with the geometric phase term (ϕ_{PB}) by addition or subtraction to generate the corresponding left-handed circular polarization (ϕ_{LCP}) and right-handed circular polarization (ϕ_{RCP}) phase profiles. Subsequently, their superposition forms the target phase profile (ϕ_{target}). As depicted in Fig. S1(b), the key to generating a vortex spot profile is

combining the original phase profile with a vortex phase term ($l\varphi$), thus breaking symmetry and forming a spiral phase distribution.

To create a multi-focal phase profile, we apply periodic sawtooth wave signal functions, $m(x)$ and $m(y)$, along the x- and y-directions, respectively, as illustrated in Fig. S1(c ~ d). The overlap of these two functions forms an asymmetric modulation matrix ($m(x)+ m(y)$), which is then superimposed onto the original phase profile. This introduces periodic phase discontinuities, breaking the circular symmetry of the original phase distribution. Consequently, the modified phase profile decomposes into multiple distinct spatial frequency components, each corresponding to a particular diffraction order, thereby producing focal spots positioned at different locations in the focal plane.

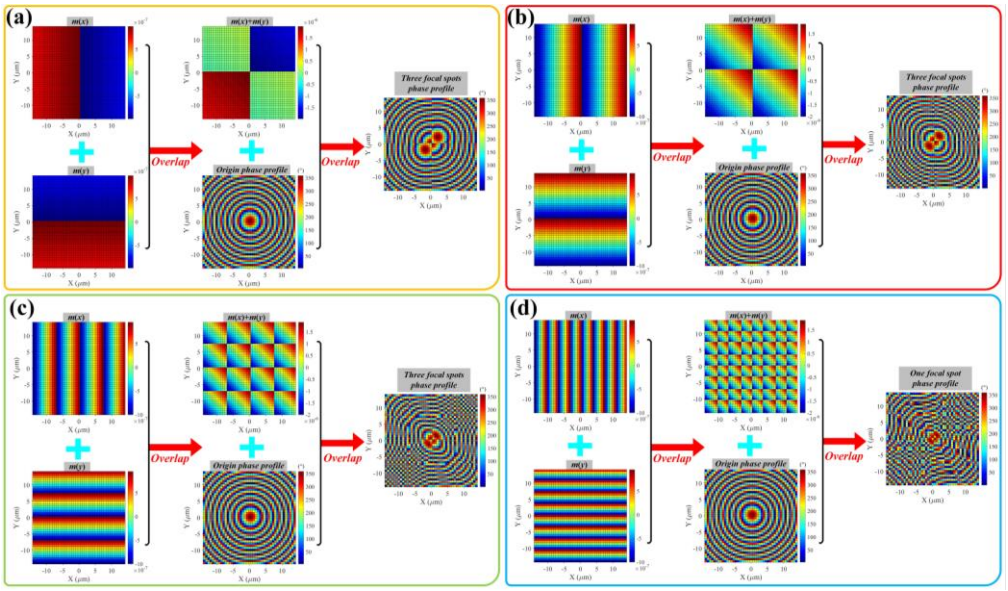

Fig. S2. Multi-focal fields generated by overlapping different sawtooth waves: (a) amplitude A = 1 μm, periods L_x = 8802.8 and L_y = 8802.8; (b) amplitude A = 1 μm, periods L_x = 70422.5 and L_y = 70422.5; (c) amplitude A = 1 μm, periods L_x = 14084.5 and L_y = 14084.5; (d) amplitude A = 1 μm, periods L_x = 28169.0 and L_y = 28169.0.

To clarify the mechanism by which these signal functions modulate the multi-focal distribution and explain how the modulation parameters amplitude (A), modulation periods (L_x and L_y) affect the focal spot distributions, we introduce additional simulation results shown in Fig. S2.

Specifically, Fig. S2 demonstrates multi-focal fields modulated by different sawtooth waves parameters. Here, amplitude (A) directly determines the spacing between generated focal

spots: larger amplitude increases the spacing, whereas smaller amplitude reduces it. Modulation periods L_x and L_y define the spatial frequency composition, thus directly influencing the number and spatial distribution of the generated focal spots. As modulation periods increase, the focal spot distribution gradually transitions from distinct multiple focal spots (Fig. S2 (a ~ c)) toward a single central focal spot (Fig. S2(d)). This phenomenon due to longer modulation periods correspond to lower spatial frequencies, causing focal spots to merge toward the center. Conversely, shorter periods introduce higher spatial frequencies, producing multiple focal spots clearly separated in space.

Additionally, Fig. S2(d) shows that the sawtooth wave signal functions $m(x)$ and $m(y)$ are rotated by 45° clockwise and 45° counterclockwise, respectively. Their overlap lead to new modulation functions, which selectively suppresses certain spatial frequency components, thereby transforming the three focal spots profile into a two focal spots profile.

In conclusion, by precisely tuning these modulation parameters, our proposed method enables versatile and highly controllable multi-focal fields, significantly expanding the functional capabilities of fiber-integrated metasurface devices.

S2. The characteristics of selected unit cells in the DP-MS.

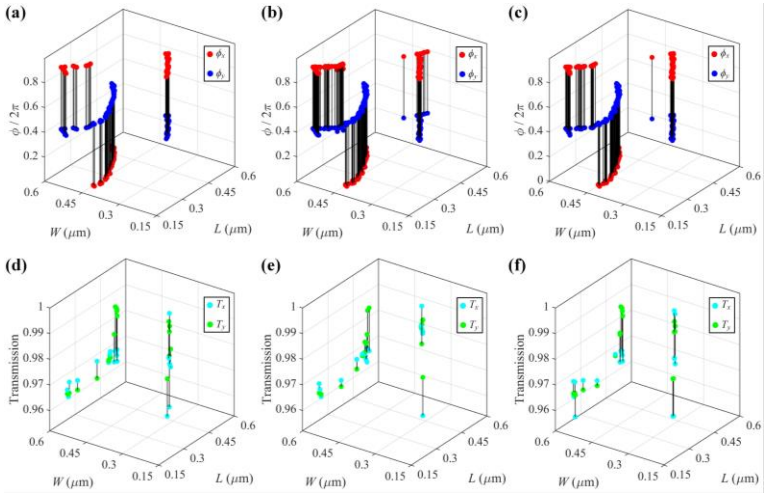

Fig. S3. Phase difference and transmission of unit cells in the OC metasurface designed to generate: (a) and (d) single focal spot, (b) and (e) vortex beam, (c) and (f) multi-focal spots.

Figure S3(a ~ c) shows the phase shifts (ϕ_x, ϕ_y) distributions of the unit cells along the x and y axes. The absolute phase difference between ϕ_x and ϕ_y satisfies $|\phi_x - \phi_y| = \pi$. The

transmission of these unit cells are shown in Fig. S3(d ~ f), where the transmittance (T_x and T_y) remains close to 100% across most parameter ranges. Tunable phase shifts and high transmission efficiency are achieved by adjusting the width (W) and length (L) of the nanobrick unit cells.

S3. Spatial range of dynamic polarization modulation.

We further analyzed the transverse optical fields at different propagation distances (ranging from 2.5 μm to 5.5 μm) to clarify the spatial range over which the dynamic polarization modulation is distinguishable. As demonstrated in Fig. S4(a ~ c), the transverse intensity distributions for three different metasurfaces (single focal spot, vortex spot, and multi-focal spots) clearly illustrate that the rotational characteristics of the focal spots are not restricted solely to the focal plane but can also be recognized across a certain axial range (from 3 μm to 5 μm). These results confirm that dynamic polarization modulation behavior and rotational features of the optical fields persist beyond the focal plane, expanding the effective operational range of the device.

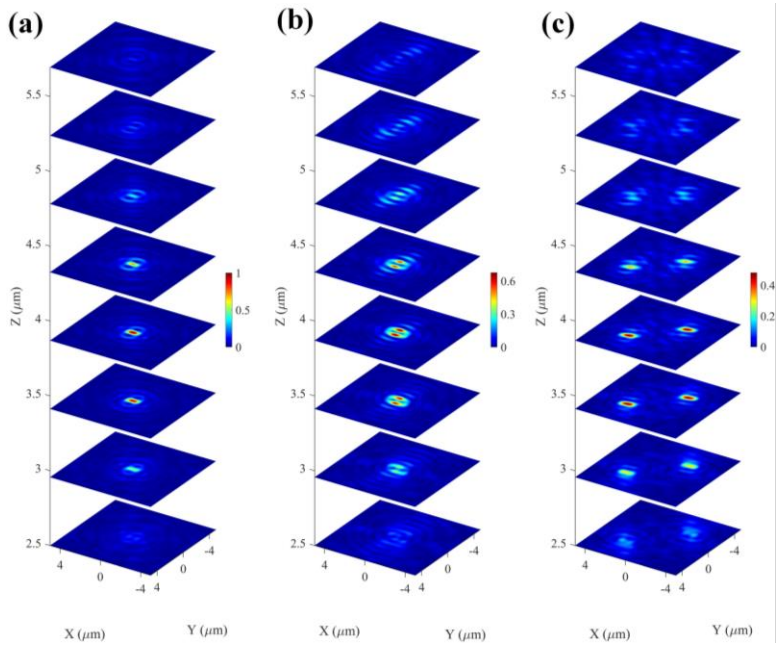

Fig. S4. Transverse optical field of three metasurfaces at different transmission distances. (a) single focal spot, (b) vortex spot, and (c) multi-focus spots.

S4. Focusing Efficiency Results.

The focusing efficiency (η) for different types of focal spots is defined as the ratio of the optical power focused at the focal plane P_{focal} to the incident optical power $P_{incident}$, expressed as: $\eta = P_{focal} / P_{incident}$.

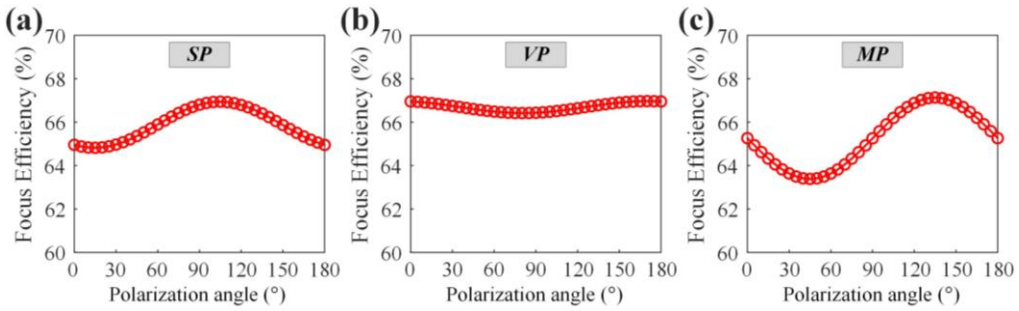

Fig. S5. Focusing efficiency of three DP-MSs. (a) single focal spot (SP), (b) vortex spot (VP), and (c) multi-focus spots (MP).

The simulation results, as shown in Fig. S4(a ~ c), depict the change of focusing efficiency with the polarization direction of the incident light. For the single focal spot (SP), the focusing efficiency varies periodically, exhibiting a clear sinusoidal dependence with polarization angles, reaching a maximum around 67% and a minimum around 64% (Fig. S5(a)). The vortex spot maintains a relatively stable focusing efficiency around 66.5% with minor fluctuations, as shown in Fig. S5(b). For multi-focus spots, the focusing efficiency exhibits a clear periodic oscillation ranging from approximately 63% to 67%, correlating with changes in polarization direction, as illustrated in Fig. S5(c).

S5. DP-MS are excited by elliptically polarized light.

To provide a comprehensive assessment of the proposed metasurface under practical conditions, we conducted additional simulations and analyses using elliptically polarized incident light on the metasurface originally designed for generating a single focal spot. Although our current metasurface design is primarily optimized for linear polarization states, these results demonstrate that it retains effective modulation capability under elliptical polarization conditions.

Specifically, we simulated elliptical polarization by superimposing two orthogonally polarized planewave sources (**S1** and **S2**). Source **S1** is fixed as an *x*-component (polarization angle = 0°, amplitude = 1, phase = 0°), and source ***S2*** is fixed along the orthogonal *y*-component (polarization angle = 90°) with amplitude $\boldsymbol{A} = \beta$ and phase = φ. The resulting elliptical polarization state can be expressed by the Jones vector:

$$\begin{pmatrix} 1 \\ \beta e^{i\varphi} \end{pmatrix}$$

The orientation angle Ψ of the major axis of the elliptical polarization relative to the *x*-axis can be calculated as:

$$\tan(2\Psi) = \frac{2\beta\cos(\varphi)}{1-\beta^2}$$

By adjusting the value of φ, we can obtain the amplitude ratio β required for generating elliptical polarization with a desired orientation angle Ψ. The optical field distributions under these elliptical polarization conditions, with orientation angles of $\Psi_1 = 30°$ and $\Psi_2 = 75°$, correspond to Fig. S6(a) and (b), respectively. In Fig. S7, we analyze the rotation angles of the focal spots as a function of the polarization angle. In Fig. S7(a), corresponding to $\Psi_1 = 30°$, the white ellipses are nearly circular, indicating that the long and short axes are approximately equal. As a result, the focal spot rotation follows a smooth, nearly linear relationship with the polarization direction. In contrast, in Fig. S7(b), corresponding to $\Psi_2 = 75°$, the white ellipses are more elongated, with one axis significantly longer than the other, which leads to a reduced linearity in the rotation compared to Fig. S7(a). However, the rotation still follows a periodic pattern, corresponding to the full rotation of the polarization directions from 0° to 180°.

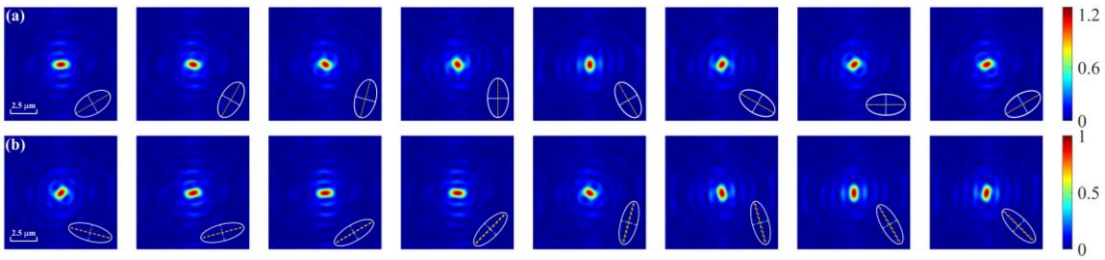

Fig. S6. Optical field rotation for the metasurface excited by elliptically polarized light with varying polarization directions: From left to right are 0°, 30°, 45°, 60°, 90°, 120°, 135°, 150°. The orientation angle (a) $\Psi_1 = 30°$ and $\Psi_2 = 75°$ (The white ellipse represents the polarization direction).

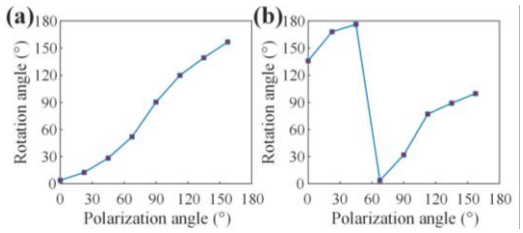

Fig. S7. Optical field rotation for the metasurface excited by elliptically polarized light varying polarization directions

S6. DP-MS designs with varied parameters: extended radius and focal length.

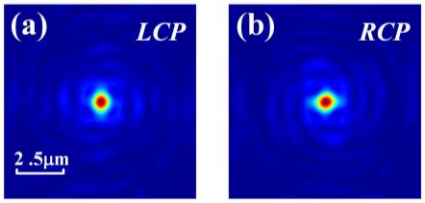

Fig. S8. Output field distribution of OC metasurface with single focal spots excited by (a) LCP and (b) RCP.

When LCP or RCP is used as incident light, only the corresponding phase profile of LCP or RCP is encoded on the unit cells, this results in a circular focal spot where the optical clock phenomenon cannot be realized, as shown in Fig. S8(a) and (b).

S7. DP-MS designs with different NA metasurfaces.

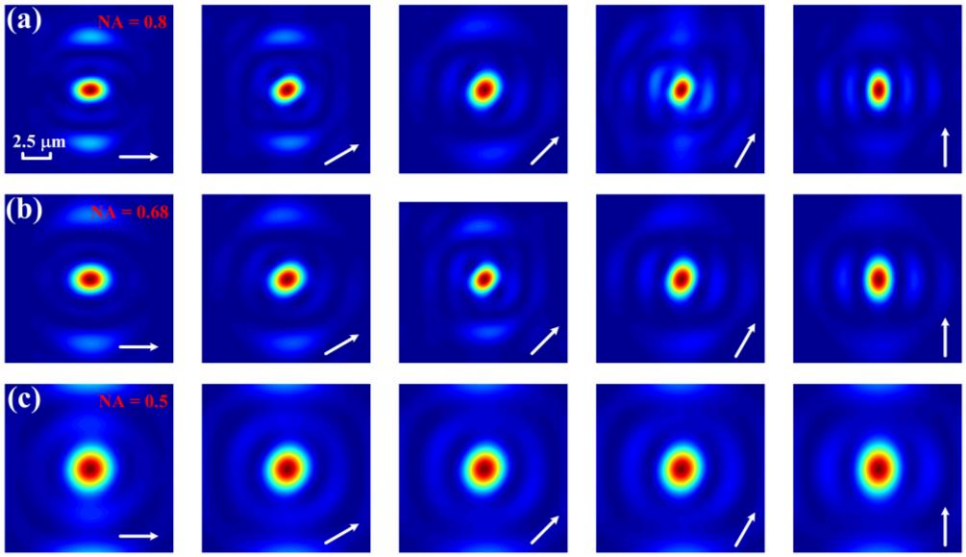

Fig. S9. Optical field rotation for the different NA metasurfaces excited by planewave varying polarization directions: From left to right are 0°, 30°, 45°, 60°, 90° (The white arrow represents the polarization direction of incident).

Results indicate that, with the metasurfaces radius held fixed (R = 14.2 μm) and the focal length increased (NA reduced), diffraction effects cause the originally elliptical focal spot to become progressively circular, thereby complicating the observation of its polarization‐driven rotation, as shown in Fig. S9.